ISSN: 2716-9227 Algerian Journal of Engineering and Technology 08 (2023) 322–332 e-ISSN: 2716-9278

Algerian Journal of Engineering and Technology

Journal homepage: https://jetjournal.org/index.php/ajet

Original Article

Stability of flowing PbLi alloy between coaxial cylinders under magnetic field

Brahim Mahfoud

Department of Mechanical, University of MOB-Bouira, Bouira, 10000, Algeria.

ARTICLE INFO

Article history:
Received 01 June 2023
Revised 28 August 2023
Accepted 04 September 2023

Keywords:
Coaxial cylinders;
Magnetic field;
PbLi alloy;
Vortex breakdown;
Stability.

ABSTRACT

In this research, numerical simulations were performed to investigate the stability of a flowing PbLi alloy (Pr = 0.032) within two coaxial vertical cylinders, while subjected to an axial magnetic field. The primary objective of this study was to analyze how the presence of the axial magnetic field affected both vortex breakdown and swirling flow phenomena. To achieve this, the governing equations, which included the Navier-Stokes equations and potential equations, were solved using the finite-volume method. The numerical simulations presented results for three aspect ratios (*A*= 1.5, 2.0, and 2.5) and three annuli (*R* = 0.9, 0.8, and 0.7). In the hydrodynamic scenario, vortex breakdown was observed close to the inner cylinder as a result of the intensified pumping effect caused by the Ekman boundary layer. The findings demonstrated that the onset of oscillatory instability was initiated by increasing the Reynolds number to a critical value. However, when a magnetic field is intensified, the vortex breakdown vanishes, and its limits will shrink. Stability diagrams were created to depict the boundaries within which a vortex breakdown bubble emerges, allowing for a visual picture of its occurrence.

1. Introduction

The PbLi 17 alloy, which is a mixture of lead (Pb) and lithium (Li) with a lithium content of 17%, has several potential applications in various industries. In nuclear Fusion, PbLi 17 alloy is often used as a coolant in nuclear fusion reactors. Its high thermal conductivity and low neutron absorption make it suitable for cooling the plasma-facing components, such as the diverter, in fusion reactors. Researchers and authors from various fields have explored its use, highlighting its exceptional capacity for neutron multiplication and its role in fusion reactors as a promising tritium breeder material. Notable scholars such as Jun et al [1] emphasized its importance in enhancing the efficiency of fusion power generation through better tritium production. A comprehensive investigation into the corrosion mechanisms of iron when exposed to liquid PbLi has been carried out by [2], utilizing a combination of first-principles calculations and molecular dynamics simulations. These findings provide fundamental insights into the dissolution corrosion behavior of Reduced Activation Ferritic/Martensitic (RAFM) steel within liquid PbLi, thereby contributing valuable foundational knowledge to this field of study In another perspective, Zinkle et al.[3] discussed the alloy's potential in advanced nuclear systems, shedding light on its inherent safety features and high thermal conductivity. The PbLi 17 alloy has been extensively studied by Edemetti et al. [4] for its role in improving the thermal-hydraulic performance of fusion blankets. These authors collectively underscore the alloy's multifaceted applications, ranging from its use as a neutron moderator to its heat transfer capabilities, solidifying its significance in shaping the future of energy generation and industrial processes.

Recent research has delved into the intriguing realm of studying the behavior of the PbLi 17 alloy when subjected

---

* *Corresponding author.* Tel.: 213699677336
E-mail address: b.mahfoud@univ-bouira.dz

Peer review under responsibility of University of El Oued.

https://doi.org/10.57056/ajet.v8i2.150

to magnetic fields, uncovering a wealth of insights into its unique properties and potential applications [5]. The interplay between the alloy's composition and the magnetic field has been meticulously investigated, shedding light on its electrical conductivity, fluid dynamics, and heat transfer characteristics [6,7]. Researchers have explored how the alloy's behavior alters under varying strengths and orientations of magnetic fields, unraveling the intricate ways in which it responds to such external influences[8,9]. These studies have not only deepened our understanding of the fundamental science behind the PbLi 17 alloy but have also illuminated its potential utility in advanced technologies such as magnetohydrodynamics (MHD) systems and fusion reactors [10,11]. By unraveling the complex interplay between the PbLi 17 alloy and magnetic fields, these recent research endeavors pave the way for innovative engineering solutions and novel applications across a spectrum of industries.

In the realm of recent research focused on the utilization of the PbLi 17 alloy under magnetic fields, several researchers have recognized that coaxial geometry is crucial for efficient heat dissipation. In studies conducted by Mahfoud et al. [12-15], a similar configuration was employed. Their investigation indicated that the introduction of a magnetic field resulted in the deceleration of the fluid in all instances, ultimately leading to the stabilization of the flow. Their findings elucidated the intricate relationship between the stabilizing flow dynamics and magnetic field orientation, shedding light on its potential for enhanced energy conversion in magnetohydrodynamics systems.

This paper aims to achieve several objectives related to the study of the bifurcation of flowing PbLi alloy between two coaxial vertical cylinders and its dependence on annular gaps, aspect ratios, and magnetic fields. The primary aim of this study is to examine and comprehend the influences of space of annulus on both the manifestation and inhibition of vortex breakdown phenomena. This analysis involves comparing three annular gaps and three aspect ratios to elucidate their influence on vortex breakdown phenomena. The second objective of the study is to determine the domain or range within which the vortex bubble appears. By identifying and defining these limits, the aim is to provide a comprehensive understanding of the conditions under which vortex breakdown occurs. Lastly, the study aims to establish the stability limits that correspond to the vortex breakdown zone as the intensity of the magnetic field grows.

2. Model, assumptions, and governing equations

A PbLi 17 alloy is used in this investigation, which is a conducting fluid with a low Prandtl number (Pr = 0.032). This fluid rotates inside the annulus of height (H). The annulus is described by $R = 1 - (r_i/r_o)$, where r_i and r_o are the inner and outer cylinder radii, respectively. The results of numerical simulations for three alternative aspect ratios, $A = H/r_o$, namely 1.5, 2.0, and 2.5, as well as three annular gaps (R = 0.9, 0.8, and 0.7), are reported. The system, which consists of fluid and solid walls, is exposed to an axial magnetic field, as shown schematically in Fig.1. The bottom disk spins at a constant angular velocity (Ω) along the z-axis, while the top disk remains motionless. Certain assumptions are made to simplify the task. These assumptions make the system analysis more manageable.

(i) The fluid under consideration is assumed to be incompressible and Newtonian in nature.

(ii) Fluid properties are considered constant throughout the study.

(iii) Negligible attention is given to Joule heating and viscous dissipation terms, as their effects are assumed to be insignificant.

(iv) The container walls are presumed to be electrically insulated, and the magnetic Reynolds number is low. is low.

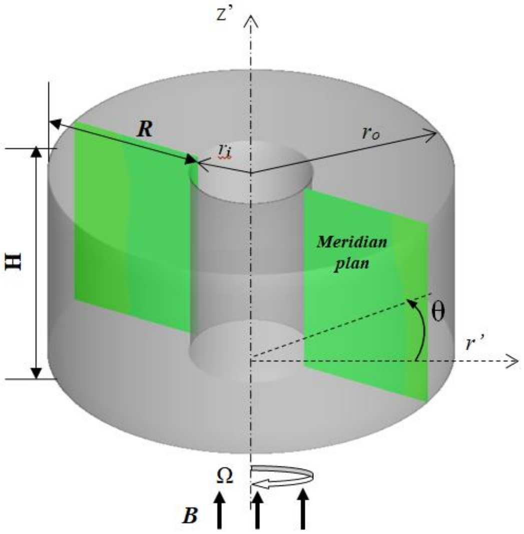

Fig 1. Flow geometry

The magnetohydrodynamic equations in this study are rendered dimensionless using the following quantities:

-Time: Normalized by the inverse of the angular velocity, 1/Ω.

-Lengths: Scaled by the outer cylinder radius, r_o.

-Velocities: Multiplied by the angular velocity and outer cylinder radius, Ωr_o.

-Pressure: Expressed in terms of the density multiplied by $\rho(\Omega r o)^2$.
-Temperature: Made dimensionless by the characteristic temperature.
-Electric potential: Given in terms of the square of the product $B_0\ \Omega r_o{}^2$.
Furthermore, the simulation assumes that the flow is laminar. Then, the dimensionless equations governing the system can be formulated.

$$\nabla . V = 0. \tag{1}$$

$$\frac{\partial V}{\partial \tau} + (V.\nabla)V + \nabla P = \frac{\nabla^2 V}{Re} + \frac{Ha^2}{Re}(V \times B) \times B \tag{2}$$

Density current:

$$J = \sigma(E + V \times B) \tag{3}$$

The electric charges:

$$E = -\nabla \Phi. \tag{4}$$

The vector velocity V is decomposed into its components in the radial direction (v_r), azimuthal direction (v_θ), and axial direction (v_z).

-The conservation of the induced electric current:

$$\nabla J = 0. \tag{5}$$

-Electric potential

$$\nabla^2 \Phi = \nabla.(V \times B) \tag{6}$$

-Lorentz force:

$$F_L = J \times B\ , \tag{7}$$

-Stream function ψ:

$$\begin{cases} v_r = 1/r\ (\partial \Psi/\partial z) \\ v_z = -1/r(\partial \Psi/\partial r) \end{cases} \tag{8}$$

-The dimensionless parameters
$\Omega r_0{}^2/\nu$: Reynolds number
$Ha = B_0 r_o \sqrt{\sigma/\rho\nu}$: Hartmann number
$A = H/r_o$: Aspect ratio
$R = 1 - r_o/r_i$: Annular gap
The simulations were initiated at the initial time (τ=0), and all calculations and analyses were carried out from this starting point. The taken boundary conditions are:
($v_r = v_\theta = v_z = 0$): in solid walls
($\partial\Phi/\partial n = 0$): all walls are electrically insulated
$v_\theta = r$: (rotating bottom disk)
$v_\theta = 0$: (stationary top disk).
$V(r,\theta,z) = V(r,\theta + 2\pi,\ z)$: the periodicity conditions

3. Calculation Conditions and Numerical Method

The numerical simulations are performed to obtain outcomes for three distinct aspect ratios: A = H/ro, specifically 1.5, 2.0, and 2.5. These simulations also consider three different annular gaps, denoted as R, with values of 0.9, 0.8, and 0.7. The simulation scenario involves an electrically conducting fluid situated between two coaxial cylinders, with a small Prandtl number (Pr = 0.032) corresponding to the PbLi 17 alloy, which is well-suited for fusion blankets. The Reynolds number range analyzed in this study spans from 1500 to 2500. Additionally, multiple magnetic intensities, characterized by Hartmann numbers, are employed to effectively suppress vortex breakdown phenomena.

The control volume method discretizes the fundamental equations, incorporating the modified central difference approximation for the diffusion terms. The solution is obtained using the tridiagonal matrix algorithm (TDMA).

Convective terms are treated using the QUICK scheme, while an implicit method is employed for temporal discretization. To handle the pressure-velocity coupling, the SIMPLER algorithm is utilized.

For this simulation, three staggered nonuniform meshes are employed, with finer meshes utilized in the regions beneath the free top and near the bottom and sidewalls for aspect ratio (A) and annular gap (R), respectively. The grids in the azimuthal direction remain uniform in all cases (Table 1). To evaluate grid convergence, simulations are conducted with various meshes for A=1.5, 2.0, 2.5, and R=0.7, 0.8, 0.9, respectively. Results are shown in Table 2, which presents the value of radiale velocity located at (r=0.5, θ=0 and z=1) confirming a good grid convergence.

Table 1 Grids utilized in the study

Annular gap, *R*	***0.7***	***0.8***	***0.9***
Meshes (*r*, θ, *z*)	70x90x70*A*	80x90x80*A*	90x90x90*A*

Table 2. Grid independence test for the case of *Re*=1500 andγ=*1.5*, and *Ha*=5.

	R=0.7	$\mathbf{v}_r$	***R=0.8***	$\mathbf{v}_r$	***R=0.9***	$\mathbf{v}_r$
Grid(*r*,*θ*, *z*)	60x90x90	0.0044	70x90x105	0.0034	80x90x120	0.00176
	70x90x105	0.0045	80x90x120	0.0037	90x90x135	0.00181
	80x90X120	0.0045	90x90x135	0.0037	100x90 x150	0.00181

4. Results and Discussion

2.1. Validation

The numerical findings achieved in this study are compared to Escudier's experimental visualizations [16]. The flow structure formed by rotating one end wall of a closed cylindrical container is visualized using the laser-induced fluorescence method. Fig. 2 depicts our findings on the right side of each figure, allowing for a direct comparison with the experimental observations. The streamlines representing various vortex breakdown regimes, including cases with one or two recirculation bubbles, for three different Reynolds number and aspect ratio combinations; (a)Re =1492 and H/R =1.5; (b) Re= 1854 and H/R =2; (c) Re =2126 and H/R =2.5.

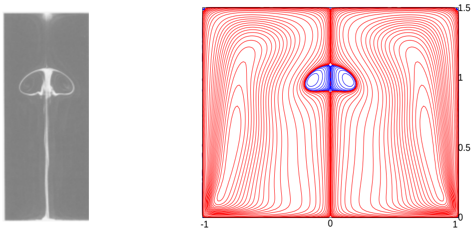

(a)Re =1492 and H/R =1.5

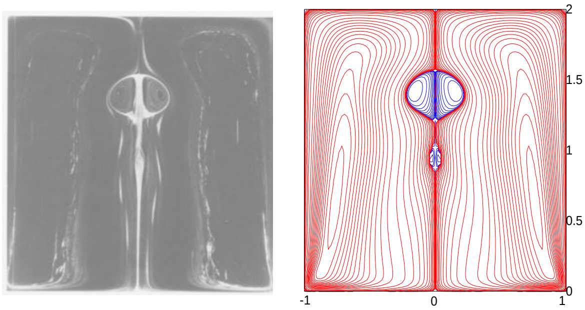

(b)Re =1854 and H/R =2.0

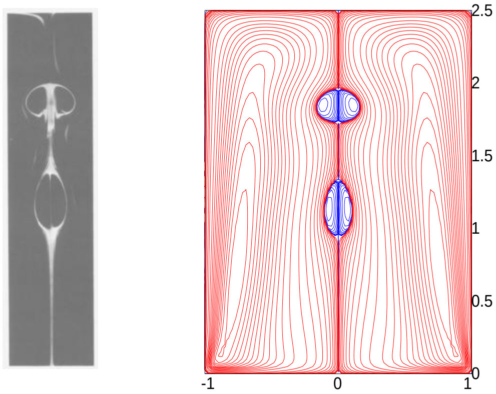

(c)Re =2126 and H/R =2.5

Fig. 2. The present results (on the right) are validated against the flow visualizations conducted by Escudier [16] (on the left).

4.2. Regime flow

For the range of Reynolds numbers examined in this study, the flow can be categorized as a steady state rather than oscillatory or turbulent. The subsequent section justifies this classification. It is well known that as the control parameter increases, a dynamic system typically progresses through different stages toward chaos. These stages include transitioning to a periodic state, entering a quasi-periodic flow, and eventually reaching turbulence. A set of numerical computations are done for each example to establish the nature of the flow regime, whether it is transient or steady-state. Fig. 3 depicts the temporal variations in axial velocity at a given monitoring point (r = 0.5, = 0, and z = 0.75), revealing flow dynamics through time. Fig. 3(a) illustrates the steady-state solutions obtained from the simulations conducted for various aspect ratios (A = 1.5, 2.0, and 2.5) at a Reynolds number of Re = 2500, with R = 0.9.

On the other hand, Fig. 3(b) presents the oscillatory nature observed in the temporal variations of axial velocity at the same monitoring point (r = 0.5, θ = 0, and z = 0.75) for Re = 2550. Increasing the Reynolds number enhances the fluid motion, leading to time-dependent flow. The degree of swirl in the flow rises as the Reynolds number increases, resulting in greater wave propagation against the flow direction [15]. Until critical Reynolds values ($Re_{cr} \approx 2545$), the flows become stable with axisymmetric contours. Beyond these critical levels, oscillatory instability occurs, especially when the annular gap is R = 0.9.

4.3 Aspect ratio effect

In order to investigate the influence of aspect ratios (A) on the characteristics of vortex breakdown, such as its occurrence, location, or suppression, the case of $Re = 2000$ with an annular gap of $R = 0.9$, considering different values of A is examined. This analysis allows us to explore how the aspect ratio affects the behavior of vortex breakdown in the system**.** Across all scenarios, a consistent observation is made: an augmentation in the rotation rate results in the acceleration of the fluid, consequently generating a vortex breakdown bubble along the inner cylinder wall. The lower disk, rotating at a higher speed, operates akin to a pump, drawing the fluid in an axial direction and expelling it outward in a spiral pattern. Within a closed annulus, this fluid rotates along the coaxial walls, spirals upward toward the stationary top disk, and then descends axially toward the rotating bottom disk. The combined effect of the spiraling flow and the conservation of azimuthal momentum leads to an amplification in swirl velocity, resulting in the formation of a concentrated vortex.

In this case, the primary and secondary recirculation bubbles form the composite of meridional flow. The streamlines in Fig. 4 confirm the presence of only one vortex breakdown for $A = 1.5$ and 2.0.

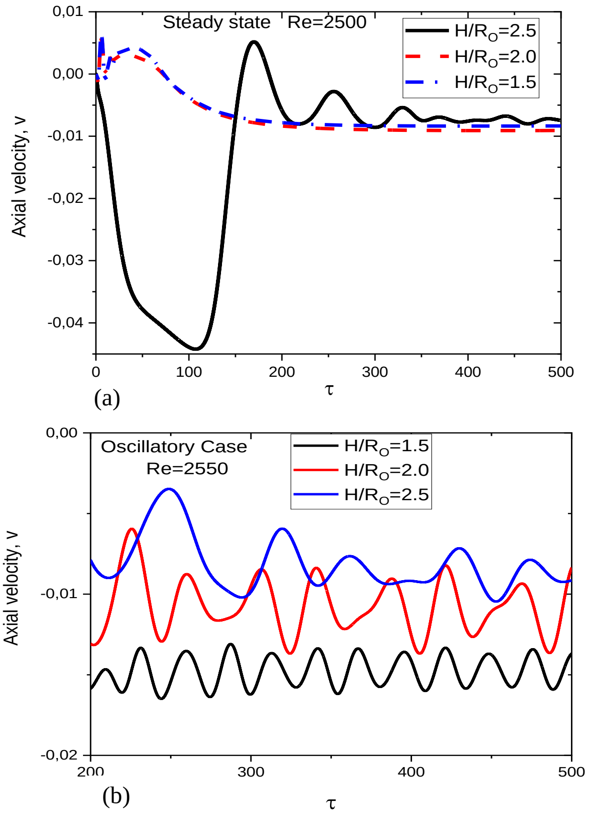

Fig 3. Evolution with a time of v_z, at the point (r = 0.5, z= 0.75).

However, for A = 2.5, no vortex breakdown is observed, as indicated by the isolines in Fig. 4. As a result, the vortices gradually diminish in size and maintain their attachment to the inner cylindrical wall. The central vortex position along the z-axis is at z = 1.101 and 1.395 for aspect ratios A = 1.5 and 2.0, respectively. Similarly, along the r-axis, the central position is identified at r = 0.167 and 0.191 for aspect ratios A = 1.5 and 2.0, respectively

Fig. 4 (lower) displays the contours of axial velocity for the three aspect ratios. In both cases (A = 1.5 and 2.), it is evident that the recirculating bubble serves as a substantial body, impeding the axial flow. When the flow encounters the vortex breakdown bubble, it undergoes a deflection, resulting in a region of reduced velocity downstream known as the wake region. Within the vortex breakdown bubble, where the axial velocity becomes zero, the effects of viscosity and inertia are negligible. It is worth noting that this behavior signifies the significance of the vortex breakdown phenomenon in altering the flow characteristics and dynamics. However, when A = 2.5, as depicted in Fig. 4, no bubble is formed. It typically occurs when the swirling motion becomes less intense.

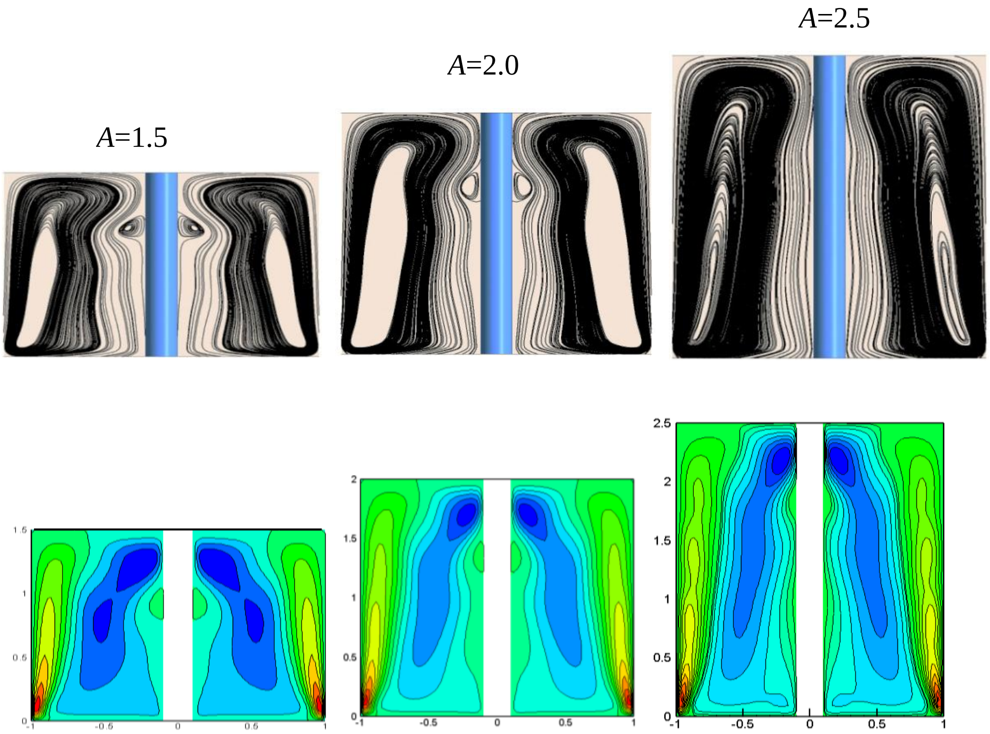

Fig 4. Case of Re=2000 at different aspect ratios A= 1.5, 2.0 and 2.

Fig.5 highlights the difference between the blue curve calculated for *R* = 0.9 in the present numerical study and the black curve experimentally constructed for *R* = 1 by Escudier [16]. This comparison helps to identify the divergence between the results obtained experimentally and those obtained through the numerical calculations performed in this study. The influence of aspect ratios on the vortex breakdown zones in the (Re, *A*) plane reveals a shift of the boundaries towards lower aspect ratio values for the annular gap (*R*=0.9), indicated by the dashed blue curve in Fig. 5. The point of intersection between the black curve (R=1.0) and the dashed blue curve (*R*=0.9) occurs at an aspect ratio, *A* of 1.2, close to Re=1000, where only a single vortex breakdown exists. This illustrates how the vortex breakdown zones are affected by the aspect ratios, with a tendency to shift towards smaller values of aspect ratio (R=0.9).

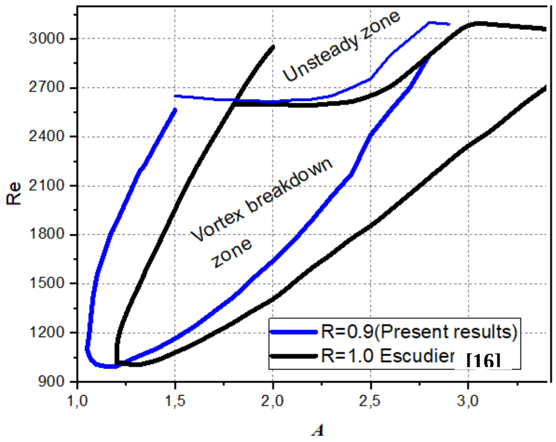

Fig 5. Comparison presents results for the *R*=0.9 with those obtained by Escudier [16]

4.4 Annular gaps effect

The occurrence and mitigation of vortex breakdown phenomena are examined in Fig.6. It specifically examines the scenario with an aspect ratio A = 1.5 and presents three distinct annular gaps (R = 0.9, 0.8, and 0.7) at three different Reynolds numbers (Re = 1500, 2000, 2500) respectively. By varying these parameters, the study aims to investigate how the annular gaps impact the flow behavior and the presence of vortex breakdown phenomena**.**

In the first column of Fig.6, the swirling flow is depicted schematically by streamlines in meridional planes (r = 0) at Re=1500 for annular gaps R=0.9, 0.8, and 0.7. When the *R* increases, a vortex emerges at *R*=0.9, with its central position along the z-axis at z=1.163. Moving to the second column of Figure 6, the case of Re=2000 is presented. When *R*=0.8, the vortex size measures 0.173. Subsequently, as the annular gap increases, the vortex size grows rapidly, reaching 0.221 when R=0.9.

The third column of Fig.6 displays streamline structures for the case of Re=2500, which differs from the previous cases. Notably, the vortex size decreases in all three cases. In the case of R=0.9, vortex breakdown occurs when *A*=2, and its size height is 1.23.

In Fig. 7, the stability limit in the (Re, *A*) plane for hydrodynamic cases (Ha=0) is presented. This diagram depicts the region where a vortex breakdown bubble occurs adjacent to the inner cylinder's sidewall for various values of the annular gap (R = 0.9, 0.8, and 0.7).

For more clarity, the curve *R*=0.9 is plotted separately in Fig. 7a. The black curve with open circle symbols corresponds to the boundary that distinguishes the vortex zone from the no-vortex zone. This boundary has been previously discussed in Fig.5, where the comparison has been made with experimental results.

The curve *R*=0.8 plotted in Fig.7b, illustrates the degree of reduction in the presence of the vortex and its displacement towards the left, indicating a movement towards lower values of the aspect ratio A = H/R.

Similarly, in the case where *R* = 0.7 (Fig.7c), the presence of the vortex also diminishes, and the limit shifts towards smaller values of the aspect ratio A. This observation indicates a trend where the vortex becomes less prominent as the aspect ratio decreases, signifying the impact of the annular gap size on the behavior of the vortex in the system.

4.5 Magnetic field effects on vortex breakdown

It is known that the magnetic field can actively suppress or weaken the formation and persistence of vortices in the swirling flow. The Lorentz forces induced by the magnetic field act on the fluid, disrupting the vortical structures and limiting their growth and development. The presence of a magnetic field can enhance the stability of the swirling flow, reducing turbulence and promoting a more organized and coherent flow pattern [6].

The Hartmann layer and the Robert layer are two distinct regions that form in swirling flows subjected to a magnetic field. The Hartmann layer is located near the walls that are perpendicular to the applied magnetic field. In this layer, a dimensionless thickness is denoted as δ⊥, which is approximately equal to 1/Ha. The magnetic field induces a Lorentz force on the conducting fluid, which opposes the fluid motion. As a result, the flow velocity decreases within the Hartmann layer. The extent and thickness of the Hartmann layer depend on the strength of the magnetic field and the properties of the fluid. The Robert layer, also known as the side layer, is situated adjacent to the Hartmann layer. This layer is characterized by a relatively higher flow velocity compared to the Hartmann layer.

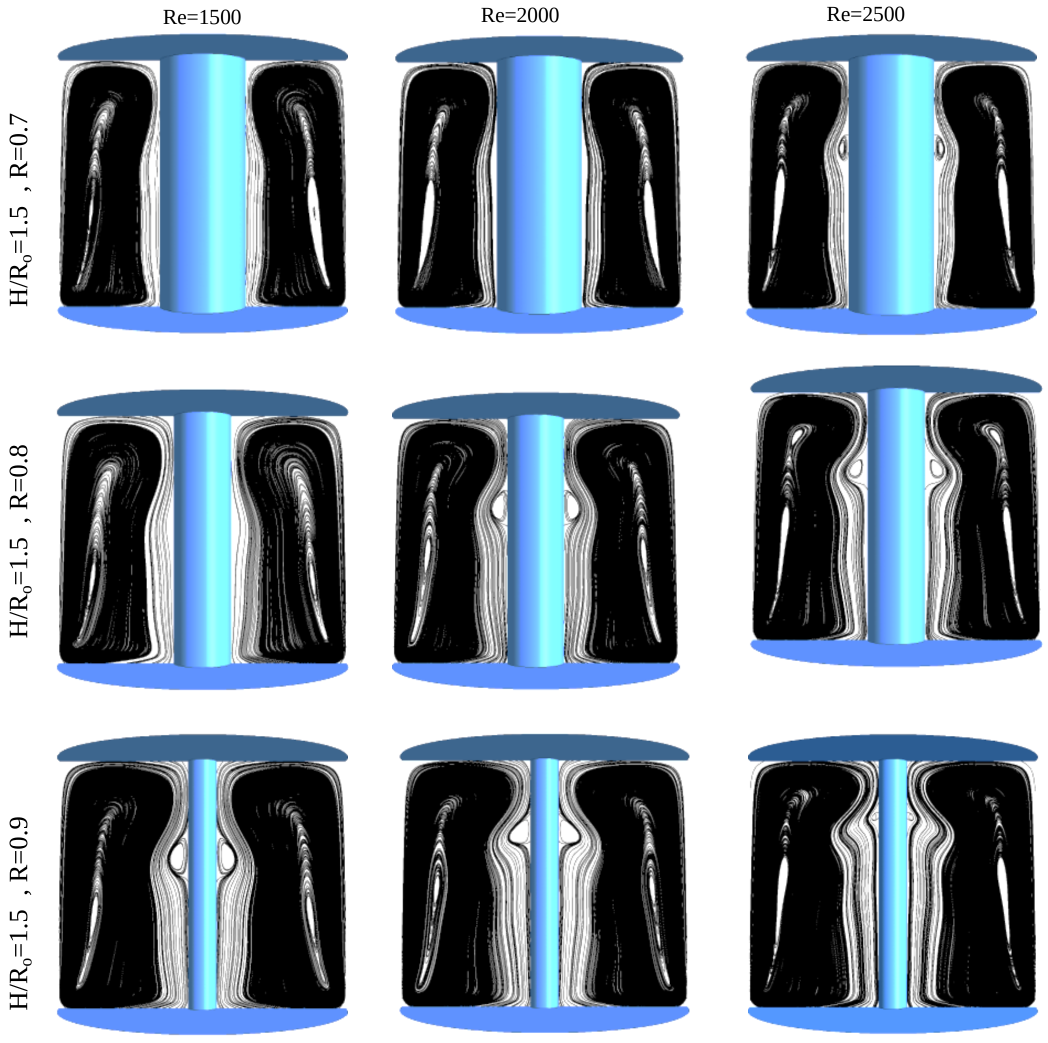

Fig 6. Stream function in case of *A*=1.5 for *R*=0.9,0.8, and 0.7 at different *Re.*

The magnitude of the axial velocity can be estimated to be on the order of $v_z \sim Re/Ha^3$. This indicates that the axial velocity is relatively weak in the presence of a magnetic field. According to the findings of Mahfoud et al. [6], it was observed that a stronger magnetic field leads to an expansion of the boundary layer and a reduction in the axial flow component.

In Fig. 8, streamlines are depicted for different Hartmann numbers (Ha = 1, 5, 8, and 10) in three distinct scenarios: Re = 1310 (left), Re = 1500 (middle), and Re = 2000 (right). These outcomes correspond to a specific setup with *A* = 1.5 at *R* = 0.9.

At Re = 1300 and Ha = 1, the central position of the vortex on the z-axis is approximately z ≈ 0.84, while on the r-axis it is 0.15. As the Ha increases to 5, the size of the vortex expands. The dimensionless length along the z-axis reduces from 0.18 at Ha = 1 to 0.11 at Ha = 5. Eventually, at a critical Hartmann number of Hacr ≈ 6.5, the vortex completely disappears.

Moving to column two in Fig. 8, the case of Re = 1500 is presented. Here, As the Hartmann number increases, the size of the vortex diminishes, eventually reaching a point where it completely vanishes at Ha = 10. In the third column, when considering Re = 2000, it can be observed that the size of vortex breakdown exhibits a noticeable augmentation as the Hartmann number (Ha) rises, and the phenomenon ceases to manifest beyond *Ha* = 10. Finally, it can be demonstrated that the size of the vortex breakdown increases with an escalating Reynolds number. Furthermore, the central positions of the vortex along the z-axis also show an upward trend as both the Reynolds number and Hartmann number are augmented.

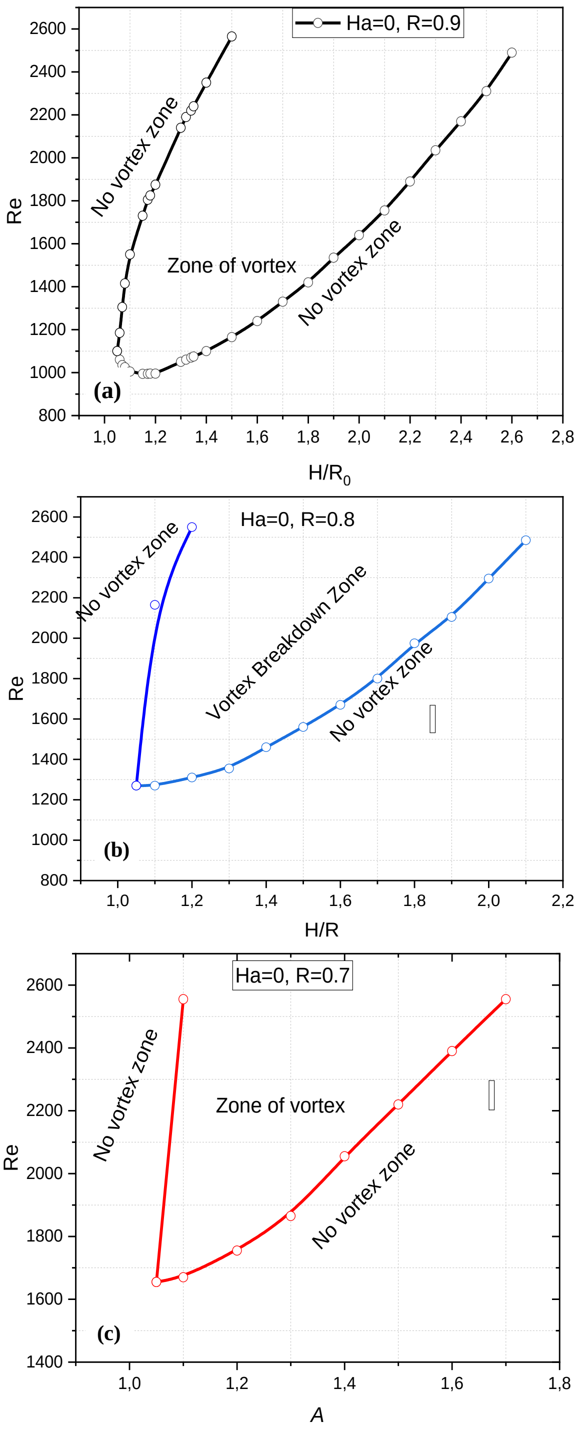

Fig 7. Stability limit in the (Re, *A*) in which a vortex breakdown occurs for (a) R=0.9, (b) 0.8, and (c) 0.7.

.

Fig.9 illustrates the impact of a magnetic field on the central position of the vortex along the z-axis. This analysis is conducted for the scenario of *A* = 2.0, with an annular gap of R = 0.9. The central position is evaluated at different Reynolds numbers ranging from 1500 to 2500. Without magnetic field, a vortex becomes noticeable at Re = 1644 and ceases to exist at Re = 2502. During the initial stage when the small vortex emerges at Re = 1644, its central position along the z-axis is situated at z = 1.27. As the Reynolds number increases up to Re = 2500, the central position gradually rises to z = 1.48. The central positions of the vortex exhibit a gradual increase when higher Hartmann numbers are applied at a constant Reynolds number. For instance, at Re = 2500, the central positions are located at z = 1.472, 1.489, and 1.506 for Ha = 0, 5, and 10, respectively. The influence of the magnetic field on the central positions of the vortex becomes more pronounced at Ha = 10, where the vortex appears around Re = 2000 and disappears at Re = 2500. Specifically, at Re = 2000 and Re = 2500, the central positions are found at z = 1.397 and 1.414, respectively. These findings demonstrate that as the Hartmann number increases, the magnetic field progressively suppresses the occurrence of vortex breakdown.

The diagram (Re, *A*) plotted in Fig.10 compares three different cases (Ha=1, 5, and 10). The purpose of this diagram is to demonstrate the influence of the Hartmann number on the vortex breakdown zones and how these boundaries shift accordingly. The black curve, represented by circle symbols, represents the boundaries for Ha = 0. As the Hartmann number increases to Ha = 5, the limits depicted by the blue curve, diminish and shift upwards compared to the Ha = 0 curve. Furthermore, for Ha = 10, the red curve demonstrates an even stronger upward shift of the vortex breakdown zone boundaries. This observation suggests that as the Hartmann number increases, the impact on vortex breakdown becomes more pronounced, resulting in a contraction of the range where vortex breakdown is observed. In other words, the decrease in the range of the boundary where the vortex breakdown occurs can be attributed to the increase in Hartmann numbers.

5. Conclusion

The study focuses on examining the stability of the swirling flow of PbLi alloy and its bifurcation in the gap between two coaxial cylinders in the presence of a magnetic field. Numerical analysis using the finite volume method was conducted to investigate various types of vortex breakdowns. The comparison of three different annular gaps (R=0.9, 0.8, and 0.7) was performed to assess flow stability. The key findings of the study are summarized as follows:

- When comparing the current findings with previous experimental results for R = 1.0, it has been observed that as the annular gap is reduced to R = 0.9, the limits of the vortex breakdown presence diminish and shift towards the left.

- The study demonstrated that decreasing the annular gap size leads to a reduction in the zone where vortex breakdown occurs.

- Findings emphasize that as the Hartmann number increases, the vortex breakdown zone diminishes in size. This suggests that higher Hartmann numbers exert a suppressive influence on the occurrence of vortex breakdown.

- In summary, this research adds to our understanding of how magnetic fields and annular gaps affect the incidence and suppression of vortex breakdown. It also highlights the possibility of manipulating the parameters of vortex breakdown occurrences using magnetic fields.

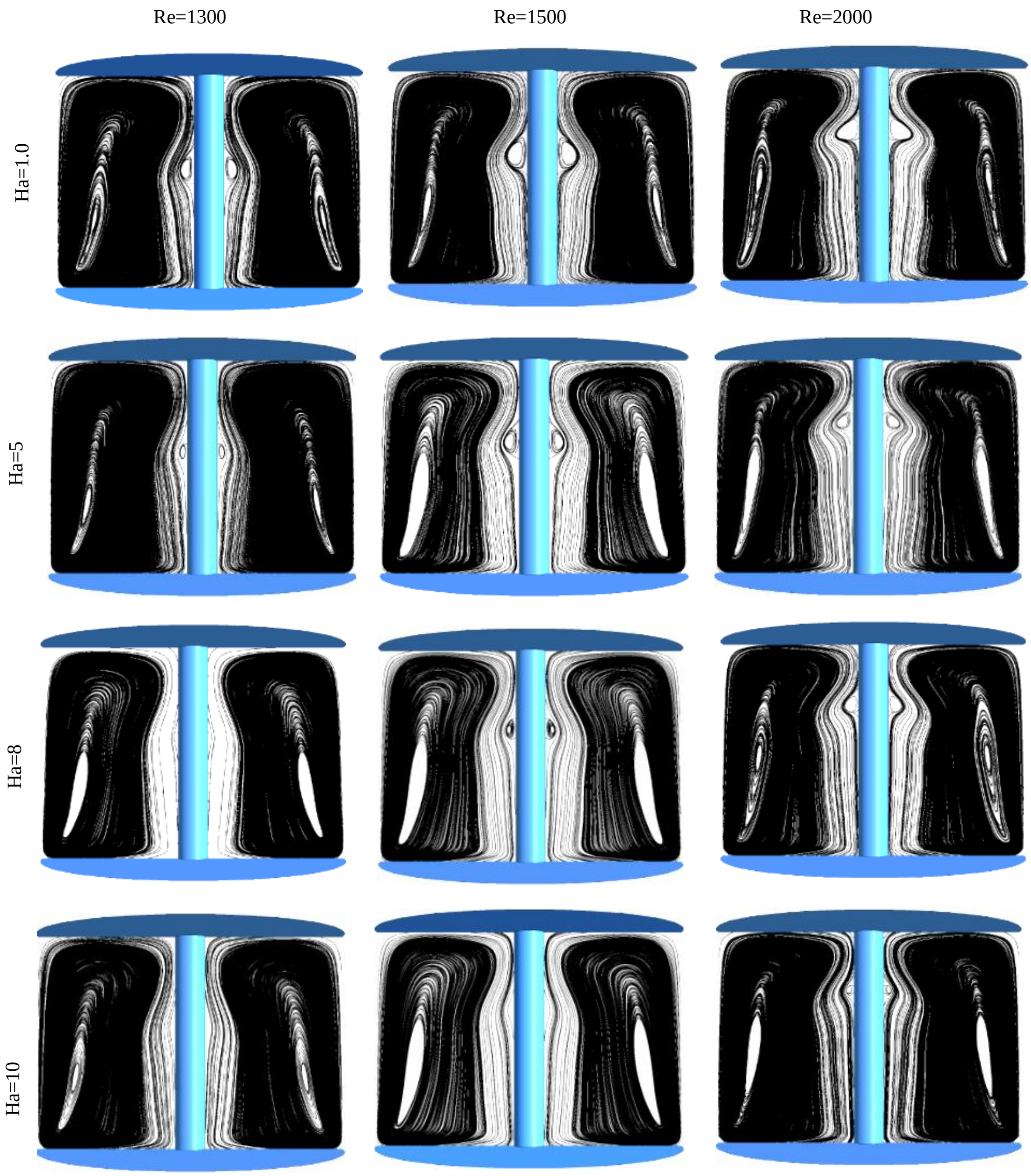

Fig 8. Streamlines in the meridional planes in three cases of Re when R=0.9 and A=1.5 for increasing Ha.

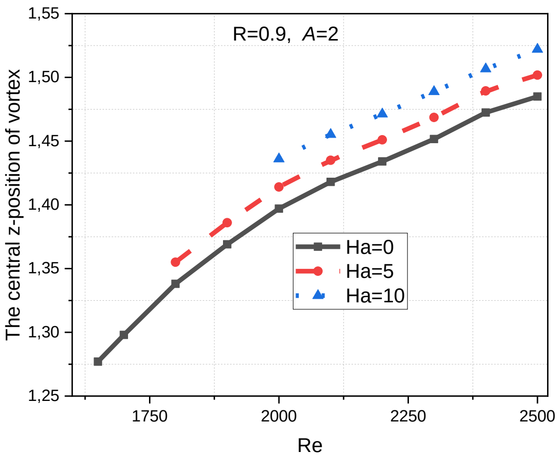

Fig. 9. Vortex-center on the z-axis

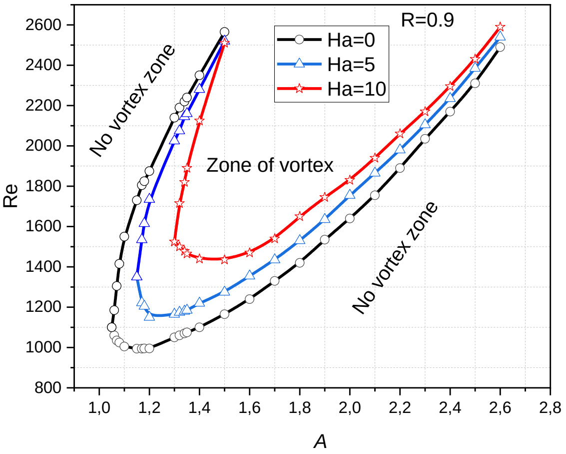

Fig.10. Diagram (*Re*–*A*) at *R=0.9*.

Nomenclature

A	aspect ratio (H/r_o)
B	magnitude of magnetic field, Tesla
E	electric charges, coulomb
F_L	Lorentz force, N
H	height of the cylinder, m
Ha	Hartmann number ($B_0 r_o\sqrt{\sigma/\rho\nu}$)
J	non-dimensional current density[-]
P	non-dimensional pressure[-]
Pr	Prandtl number ($Pr=\nu/\alpha$)
R	non-dimensional annular gap
Re	Reynolds number($\Omega r_0{}^2/\nu$)
Re_m	magnetic Reynolds $Re_m = \mu_0\sigma\Omega R_o{}^2$
r_o	radius of the outer cylinder, m
r_i	radius of the inner cylinder, m
V	velocity vector
α	thermal diffusivity of the fluid, m^2/s
ν	kinematic viscosity of the fluid, m^2/s
ρ	density of the fluid, kg/m^3
σ	electric conductivity, Ω /m
Φ	non-dimensional electric potential
Ω	angular velocity, rad/s
Ψ	non-dimensional stream function

Acknowledgements

The authors gratefully acknowledge the support of the General Directorate of Scientific Research and Technological Development (DGRSDT - Algeria).

Conflict of Interest

The author declares that they have no conflict of interest

References

1. Jun J, Unocic K.A , Lance MJ , Meyer HM , Pint BA. Compatibility of FeCrAlMo with flowing PbLi at 500°-650 °C. *Journal of Nuclear Materials*,2020, 528: 151847, https://doi.org/10.1016/j.jnucmat.2019.151847
2. Jiang Z, Zheng M, Jiang M, Xin J. The influence of crystal orientation on corrosion behavior of iron in liquid PbLi Wenyi Ding. *Journal of Nuclear Materials*, 2018, 509 : 212-217, https://doi.org/10.1016/j.jnucmat.2018.06.039
3. Zinkle J, Terrani KA , Snead LL . Motivation for utilizing new high-performance advanced. materials in nuclear energy systems, *Current Opinion in Solid State and Materials Science*, 2016, 20: 401-410, https://doi.org/10.1016/j.cossms.2016.10.004
4. Edemetti F, Piazza I.Di , Del Nevo A . Caruso G. Thermal-hydraulic analysis of the DEMO WCLL elementary cell: BZ tubes layout optimization, *Fusion Engineering and Design*,2020,160: 111956, https://doi.org/10.1016/j.fusengdes.2020.111956
5. Gonzalez M , Garcia JM , Kravalis K . Chemical compatibility of bulk alumina in flowing PbLi alloy under magnetic field, *Fusion Engineering and Design*, 2021,170: 112704 doi. /10.1016/j.fusengdes.2021.112704
6. Mahfoud B. Effects of an Axial Magnetic Field on Vortex Breakdown and Fluid Layer, *Journal of Applied Fluid Mechanics* ,2021, 14: 1741–1753, https://doi.org/10.47176/jafm.14.06.32585
7. Smolentsev S, Li FC , Morley N , Ueki Y, Abdou M , Sketchley T. Construction and initial operation of MHD PbLi facility at UCLA, Fusion Engineering and Design, 2013, 88: 317-326 https://doi.org/10.1016/j.fusengdes.2013.03.018

8. Smolentsev S, Saedi S, Malang S, Abdou M. Numerical study of corrosion of ferritic/martensitic steels in the flowing PbLi with and without a magnetic field, *Journal of nuclear materials*, 2013, 432: 294-304 https://doi.org/10.1016/j.jnucmat.2012.08.027
9. Li FC, Sutevski D, Smolentsev S, Abdou M. Experimental and numerical studies of pressure drop in PbLi flows in a circular duct under non-uniform transverse magnetic field, *Fusion Engineering and Design*, 2013, 88 : 3060-3071, https://doi.org/10.1016/j.fusengdes.2013.08.006
10. Smolentsev S, Li FC, Morley N, Ueki Y, Abdou M . Construction and initial operation of MHD PbLi facility at UCLA, *Fusion Engineering and Design*, 2013, 88 : 317-326, https://doi.org/10.1016/j.fusengdes.2013.03.018
11. Mistrangelo C, Bühler L. Magnetohydrodynamic flows in liquid metal blankets for fusion reactors, *PAMM · Proc. Appl. Math. Mech* 2017, 17: 115 – 118, https://doi.org/10.1002/pamm.201710033
12. Mahfoud B. Magnetohydrodynamic effect on vortex breakdown zones in coaxial cylinders, *European Journal of Mechanics-B/Fluid*, 2021, 89: 445–457. doi.org/10.1016/j.euromechflu.2021.07.007 0997-7546
13. Benhacine H, Mahfoud B., Salmi M. Stability of an Electrically Conducting Fluid Flow between Coaxial Cylinders under Magnetic field." *Journal of Applied Fluid Mechanics*, 2022, 15 : 1741-1753, DOI: 10.47176/JAFM.15.02.33050
14. Mahfoud B, Laouari A, Hadjadj A, Benhacine H. Counter-rotating flow in coaxial cylinders under an axial magnetic field. *European Journal of Mechanics-B/Fluids*, 2019; 78: 139-146. doi.org/10.1016/j.euromechflu.2019.06.009
15. Mahfoud B., Benhacine H., Laouari A., Bendjaghlouli A. Magnetohydrodynamic Effect on Flow Structures Between Coaxial Cylinders Heated from Below, *Journal of Thermophysics and Heat Transfer*, 2019, 34(2): 1-10. https://doi.org/10.2514/1.T5805.
16. Escudier M. Observations of the flow produced in a cylindrical container by a rotating endwall, *Experiments in Fluids*, 1984, 2: 189–196.

Recommended Citation

Mahfoud B. Stability of flowing PbLi alloy between coaxial cylinders under magnetic field. *Alger. J. Eng. Technol. 2023*, 8(2): 322-332. DOI: https://doi.org/10.57056/ajet.v8i2.150